ARTICLES

Meson-exchange and quark-gluon transitions in the $\bar{p}p \rightarrow \bar{\Lambda}\Lambda$ process

J. Haidenbauer
Department of Physics and Mathematical Physics, University of Adelaide, Adelaide 5001, Australia

K. Holinde, V. Mull, and J. Speth
Institut für Kernphysik, Forschungszentrum Jülich GmbH, W-5170 Jülich, Germany
(Received 31 March 1992)

Different $\bar{p}p \rightarrow \bar{\Lambda}\Lambda$ transition mechanisms [$K+K^*$ exchange, K exchange only, and quark-gluon exchange ($^3S_1$ version)] are investigated in a full coupled-channel ($\bar{p}p, \bar{\Lambda}\Lambda$) calculation. The elastic part of the $\bar{p}p$ and $\bar{\Lambda}\Lambda$ interactions has been derived from a one-boson-exchange version of the Bonn NN potential and a corresponding extension to the hyperon-nucleon case whereas the annihilation part is taken into account by phenomenological optical potentials. As expected, results for spin observables differ substantially for the different transition models. It turns out that resulting polarizations and spin correlation parameters are quite sensitive to variations in the initial- and final-state interactions whereas spin-transfer parameters are much more stable in this regard. Therefore, the latter observables, especially the depolarization D_{nn}, can be used to discriminate between various transition scenarios.

PACS number(s): 24.85.+p, 13.75.Cs, 21.30.+y, 25.43.+t

I. INTRODUCTION

Within the past few years the experiments done by the PS-185 Collaboration at LEAR (CERN) have greatly enhanced our knowledge on the hyperon production process $\bar{p}p \rightarrow \bar{\Lambda}\Lambda$. This achievement was parallelled (though not quite matched) by a vivid development on the theoretical side. Here basically two approaches have been advocated: the traditional meson-exchange picture where the $\bar{p}p \rightarrow \bar{\Lambda}\Lambda$ transition is mediated by the exchange of strange mesons (K, K^*, K_2^*, etc.) [1–6] and the constituent-quark model where the $\bar{\Lambda}\Lambda$ pair is produced from the $\bar{p}p$ state via the annihilation of a $\bar{u}u$ pair and the subsequent creation of an $\bar{s}s$ pair [1,7–13].

In general with both approaches a qualitative reproduction of the bulk of the existing data can be achieved. On the other hand, several theoretical aspects remained controversial and are, in fact, still a topic of on-going discussions. For example, in the case of meson-theoretical models the relative importance of the exchange of the various K mesons could not be clarified. While Kohno-Weise [1] and LaFrance-Loiseau [2] needed only the lightest one [$K(495)$ ($J^P=0^-$)], $K^*(892)$ ($J^P=1^-$) was included in the investigations of Niskanen [3], the Nijmegen group [4], and the Bonn-Jülich group [6], and claimed to be important for the success of the pertinent models. Tabakin and Eisenstein [5] also considered the heavy $K_2^*(1430)$ ($J^P=2^+$) and found it to be significant even for very low energies. Controversies in the case of models based on quark-gluon dynamics centered around the issue of which quantum numbers one should preferably attribute to the fundamental quark annihilation-creation vertex [9,11,12].

Of course, there also have been topics where most of the authors agreed. For example, it is generally believed that meson-exchange potentials and quark-gluon-based models can provide a description of the data of more or less equally good quality, despite their rather different physical ingredients. Furthermore, it has been found that there is a strong sensitivity of the $\bar{p}p \rightarrow \bar{\Lambda}\Lambda$ results to distortions from the initial ($\bar{p}p$) and final ($\bar{\Lambda}\Lambda$) states.

Indeed it is this influence of the initial-state interaction (ISI) and final-state interaction (FSI) which very much obscures our theoretical understanding of the $\bar{p}p \rightarrow \bar{\Lambda}\Lambda$ process. In the domain where $\bar{\Lambda}\Lambda$ production sets in the $\bar{p}p$ system is already at rather high energies where the commonly used model descriptions are afflicted by theoretical uncertainties [6]. Moreover, in many cases the $\bar{p}p$ interaction has been simply uncritically extrapolated from corresponding investigations at low ($\bar{p}p$) energies. The interaction in the $\bar{\Lambda}\Lambda$ channel provides an even bigger problem as no experimental information on it is available, although the elastic part can be inferred from theoretical investigations on the nucleon-lambda ($N\Lambda$) system by G-parity arguments.

As a consequence of these uncertainties the available theoretical studies of the $\bar{p}p \rightarrow \bar{\Lambda}\Lambda$ reaction differ considerably with regard to how these initial- and final-state distortions are taken into account. Full coupled-channel treatments, for example, have been attempted mostly by those groups which had developed hyperon-nucleon models before that could be utilized to constrain the interaction in the $\bar{\Lambda}\Lambda$ channel [3,4,6]. Some calculations were done in a distorted-wave Born approximation (DWBA) approach [1,2,11]. Several authors work in a plane-wave Born approximation (PWBA) [5,7–10,12,13] and account for effects of the ISI and FSI by multiplying the transi-

tion Born amplitude with energy- and J-dependent functions,

$$T_J^{\bar{p}p\to\bar{\Lambda}\Lambda}=\sqrt{S_J^{\bar{p}p}(E)}\,T_{J,\text{Born}}^{\bar{p}p\to\bar{\Lambda}\Lambda}(E)\sqrt{S_J^{\bar{\Lambda}\Lambda}(E)}\ , \qquad (1.1)$$

or absorb them simply into the coupling constant. While this procedure may have some justification at very high energies, it appears to be a rather crude approximation at those energies in the threshold region where most of the high-quality data of the PS-185 Collaboration have been taken (as we will demonstrate later).

Thus, since most of the investigations have been carried out in different frameworks and with different assumptions for the $\bar{p}p$ and $\bar{\Lambda}\Lambda$ interactions it is difficult to compare them and to draw reliable conclusions. This rather unsatisfactory situation motivated us to the present study in which we want to reexamine some of the controversial issues addressed above in a well-defined and consistent framework.

We present here a detailed comparison of different transition mechanisms proposed for the $\bar{p}p\to\bar{\Lambda}\Lambda$ reaction. In particular, we consider a model based on K as well as K^* exchange, one with only K exchange, and finally a transition potential obtained in the constituent-quark model. For all three cases we use exactly the same (initial) $\bar{p}p$ interaction and also the same form for the interaction in the (final) $\bar{\Lambda}\Lambda$ channel. In order to account for the distortion effects from the ISI and FSI exactly we work in a coupled-channel approach throughout. This consistent framework allows us to thoroughly check the so far reported conjectures and findings on the $\bar{p}p\to\bar{\Lambda}\Lambda$ process. Our main aim, however, is to look for observables which show a significant sensitivity to particular transition mechanisms and therefore could be used to discriminate between the competing theoretical models of the $\bar{p}p\to\bar{\Lambda}\Lambda$ reaction.

The starting point for the present study is our earlier investigation on the $\bar{p}p\to\bar{\Lambda}\Lambda$ transition [6]. From there we take over the interaction models in the $\bar{p}p$ and $\bar{\Lambda}\Lambda$ channels. These interactions are shortly reviewed again in Sec. II. Furthermore, we will use the results based on a transition potential with K and K^* exchange, also given in Ref. [6]. The two other transition models, based on K exchange (only) and on quark-gluon dynamics, respectively, are introduced here and described also in Sec. II.

A detailed analysis of $\bar{p}p\to\bar{\Lambda}\Lambda$ predictions resulting from the three different transition models is given in Sec. III. Anticipating our main results, we confirm the general insensitivity of the cross sections to the particular transition mechanism and the strong dependence of the polarizations (as well as most of the spin correlation parameters) on both the transition mechanism and the ISI and FSI. However, we also find remarkable differences in the predictions for spin-transfer parameters, which are only weakly influenced by initial- and final-state distortions and therefore should be suitable for discriminating between different transition scenarios. The paper ends with a summary in Sec. IV.

II. THE MODELS

Our investigations are carried out in a coupled-channel approach. In this way two-body unitarity is automatically preserved (in the absence of annihilation) and the distortion effects from the initial- as well as final-state interactions are taken into account exactly. This is important in view of the well-known sensitivity of the $\bar{p}p\to\bar{\Lambda}\Lambda$ reaction to initial- and final-state distortions. The formalism we use has been described in some detail in our previous paper [6]. It now remains to specify the interaction models used in the various channels.

A. Interactions in the $\bar{p}p$ and $\bar{\Lambda}\Lambda$ channels

For the interactions in the diagonal channels ($\bar{p}p\to\bar{p}p$, $\bar{\Lambda}\Lambda\to\bar{\Lambda}\Lambda$) we utilize the potentials of Ref. [6]. There the elastic part of the $\bar{p}p$ interaction has been taken to be the G-parity transform of an energy-independent one-boson-exchange (OBE) version (OBEPF of Ref. [14]) of the Bonn NN potential [15]. Analogously, the corresponding interaction in the $\bar{\Lambda}\Lambda$ channel has been derived from our hyperon-nucleon (YN) potential [16]. For both cases the G-parity transform can be done in a clearcut manner, i.e., all occurring coupling constants but also form-factor parameters can be taken over from the NN and YN sectors, respectively, and therefore no additional short-range prescriptions have to be introduced.

The annihilation part of both the $\bar{p}p$ and $\bar{\Lambda}\Lambda$ interaction is parametrized by means of a phenomenological energy and isospin-independent optical potential of Gaussian form:

$$V_{\text{opt}}^{\bar{p}p,\bar{\Lambda}\Lambda}=\Big[(U_C+iW_C)+(U_{LS}+iW_{LS})\mathbf{L}\cdot\mathbf{S} +(U_T+iW_T)\boldsymbol{\sigma}_1\cdot\mathbf{r}\,\boldsymbol{\sigma}_2\cdot\mathbf{r}\Big]e^{-r^2/2r_0^2}\ . \qquad (2.1)$$

For $\bar{p}p$, the coupling strengths (U_i, W_i) and the range parameter r_0 have been determined independently from the $\bar{\Lambda}\Lambda$ channel by a fit to the total, integrated elastic, and charge-exchange $\bar{p}p$ cross sections in the energy range relevant for $\bar{\Lambda}\Lambda$ production. In this paper, we will use two alternative models, one (B) without and the second (C) with a tensor-type term. With the parameter sets shown in Table I, a satisfactory overall reproduction of available $\bar{N}N$ data could be achieved (cf. Ref. [6] in the case of model B).

The corresponding strength and range parameters in the $\bar{\Lambda}\Lambda$ channel represent the only free parameters of our

TABLE I. Parameters of the phenomenological optical potential in the $\bar{p}p$ channel for the different initial-state interaction models B and C described in the text.

	B	C
U_C	−1260 MeV	−3938 MeV
W_C	−4331 MeV	−6300 MeV
U_{LS}	−1575 MeV	−1575 MeV
W_{LS}	394 MeV	394 MeV
U_T		−788 MeV fm^{-2}
W_T		−788 MeV fm^{-2}
r_0	0.40 fm	0.38 fm

model and are to be determined essentially by a fit to the $\bar{p}p \to \bar{\Lambda}\Lambda$ cross sections.

B. $\bar{p}p \to \bar{\Lambda}\Lambda$ transition interactions

We consider three different models for the transition interaction (Fig. 1): a model based on K as well as K^* exchange [Fig. 1(a)], one with only K exchange [Fig. 1(b)], and finally a model motivated by quark-gluon dynamics [Fig. 1(c)]. Since transition interactions of the first kind have already been used in a previous paper [6], we will make use of the results reported there. In particular, we will utilize model I of Ref. [6] for the present investigation.

It has been noted in Ref. [6] that the K and K^* mesons play the same role in the ΛN and ΣN interactions as π and ρ in the usual NN potential; their central components add coherently whereas the tensor components have opposite signs. For the antibaryonic systems considered here the signs of the π- and K-meson contributions are reversed (due to G-parity or charge conjugation, respectively). As a consequence, K and K^* exchange interfere destructively in the central part of the $\bar{p}p \to \bar{\Lambda}\Lambda$ transition interaction but add coherently in the tensor part. Therefore, the omission of K^* leads to an enhancement of transitions in states dominated by the central forces, however, it reduces considerably tensor-type transitions. Since the latter dominate the $\bar{p}p \to \bar{\Lambda}\Lambda$ process (cf. Ref. [6]), the strength of the K exchange had to be increased in order to get again a good description of the data. We achieved that by increasing the cutoff mass $\Lambda_{N\Lambda K}$ from 1.2 GeV (used in the $K+K^*$ model and in Ref. [16]) to 1.7 GeV.

In the past few years a large variety of so-called QCD-inspired models for the $\bar{p}p \to \bar{\Lambda}\Lambda$ transition have been proposed [1,7–13]. Their common starting point is the basic transition mechanism shown in Fig. 2, where a $\bar{u}u$ pair is annihilated and subsequently an $\bar{s}s$ pair is created. Hadronic matrix elements are then calculated from the basic transition operators by using SU(6) wave functions for the involved baryons.

However, while in some of these investigations it is assumed that the annihilation or creation process goes along with the emission or absorption of a gluon [Fig. 2(a)], others assume that this process takes place into and out of the vacuum [Fig. 2(b)]. Corresponding to the

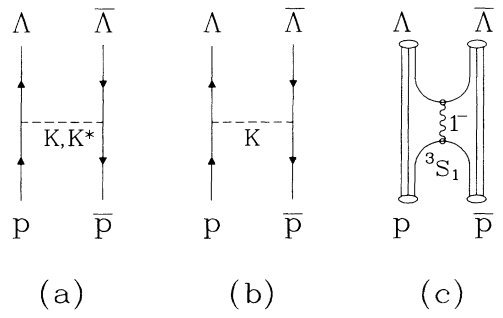

FIG. 1. Transition mechanism for the $\bar{p}p \to \bar{\Lambda}\Lambda$ process based on (a) $(K+K^*)$-meson exchange, (b) K-meson exchange, and (c) the constituent-quark model ($^3S_1$ version).

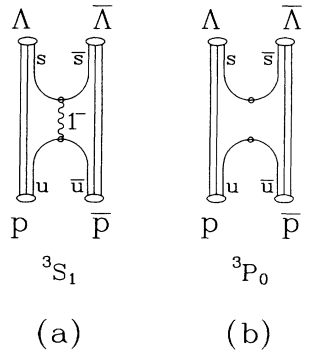

FIG. 2. The annihilation of the $\bar{u}u$ pair and the creation of the $\bar{s}s$ pair in the constituent-quark model can proceed (a) via one-gluon exchange ($^3S_1$ version) or (b) with the quantum numbers of the vacuum ($^3P_0$ version).

quantum numbers at the annihilation or creation vertex these two different approaches are commonly labeled as $^3S_1$ or $^3P_0$ models, respectively. Both approaches have been extensively employed in studies of various hyperon-antihyperon production channels. On the other hand, there is still a controversy in the literature about which of the two models actually compares better with experiment [9,12]. Recently it has also been proposed to employ a superposition of the $^3S_1$ and $^3P_0$ models rather than to consider them as two alternatives [11].

In the present study we are, however, more interested in the common features of these transition potentials derived from quark-gluon dynamics rather than in their differences. One of their shared characteristics is that the transition to $\bar{\Lambda}\Lambda$ can take place only in a spin-triplet state because of the Pauli principle. Since the isospin of the two spectator quarks is zero their spin must also be zero and therefore the spin of the $\bar{\Lambda}\Lambda$ state must be the same as the spin of the created pair of quarks, namely, $S=1$. Another common feature concerns the tensor force. The nondiagonal transition (potential) matrix elements $(V^{\bar{p}p \to \bar{\Lambda}\Lambda}_{L,L'}$, with $L \neq L')$ are, in general, considerably smaller than the ones obtained in the meson-exchange picture, or even identical to zero in the (commonly used approximative version of the) $^3S_1$ model [9].

We want to consider here the more extreme case and employ a model of the latter kind. For that purpose we utilize the model proposed in Ref. [1]. A detailed derivation can be found in Ref. [17]. Here we quote only the final form of the transition potential, after all the quark-gluon degrees of freedom have been integrated out. It reads

$$V^{\bar{p}p \to \bar{\Lambda}\Lambda} = \frac{4}{3} 4\pi \frac{\alpha}{m_G^2} \delta_{S1} \delta_{TO} \left[\frac{3}{4\pi \langle r^2 \rangle} \right]^{3/2} e^{-3r^2/4\langle r^2 \rangle}, \quad (2.2)$$

where S and T are the total spin and isospin, respectively, $\langle r^2 \rangle$ is the mean square radius associated with the quark distribution in the proton or Λ hyperon, and α/m_G^2 represents an effective (quark-gluon) coupling strength with m_G being an effective gluon mass. We took over the

value $\langle r^2\rangle^{1/2}=0.55$ fm from Ref. [1]. The effective coupling strength $\alpha/m_G^2\simeq 0.15$ fm,^{2} which was used in the DWBA calculation of the $\bar{p}p\to\bar{\Lambda}\Lambda$ process, turned out to be too small in our coupled-channel treatment to allow a reasonable reproduction of the $\bar{p}p\to\bar{\Lambda}\Lambda$ data over a wider energy range. We found a value of $\alpha/m_G^2\simeq 0.25$ fm^2 to be more appropriate. This transition model will be abbreviated by QG in the following.

III. RESULTS

In this section we want to carry out a thorough comparison of various $\bar{p}p\to\bar{\Lambda}\Lambda$ observables resulting from the three different transition models described in the previous sections. In all cases exactly the same initial-state interaction (B) and the same form for the final-state interaction is employed. The seven open parameters occurring in the annihilation part of the $\bar{\Lambda}\Lambda$ interaction [Eq. (2.1)] have been determined for each of the three models by a best fit to the total and differential $\bar{p}p\to\bar{\Lambda}\Lambda$ cross sections in the range $p_{\rm lab}\le 1700$ MeV/c. Their values are compiled in Table II. The other observables considered here, in particular, the spin-correlation and spin-transfer parameters, are genuine predictions of the interaction models. All these observables are defined in the Appendix. The sensitivity of the results to ISI or FSI effects is demonstrated, for the quark-gluon model, by employing the alternative initial-state interaction model C, see Table I.

A. Cross sections

Total $\bar{p}p\to\bar{\Lambda}\Lambda$ cross sections calculated from the three models are compared with empirical data [18–21] in Fig. 3(a) (near threshold) and Fig. 3(b) (for momenta up to $p_{\rm lab}=1900$ MeV/c). Evidently, in the threshold region, all model predictions are very similar and moreover in excellent agreement with experiment. Also at higher energies ($p_{\rm lab}\le 1750$ MeV/c) the results for the three models are qualitatively the same and give a reasonable description of the data.

Differential cross sections are shown in Fig. 4. For $\bar{p}$ momenta $p_{\rm lab}\le 1476$ MeV/c the predictions are of comparable quality. They are also in nice agreement with the experiments [18,19] (except for 1476.5 MeV/c, where there seems to be a normalization problem with the data [22]). With increasing energy the QG model and the two

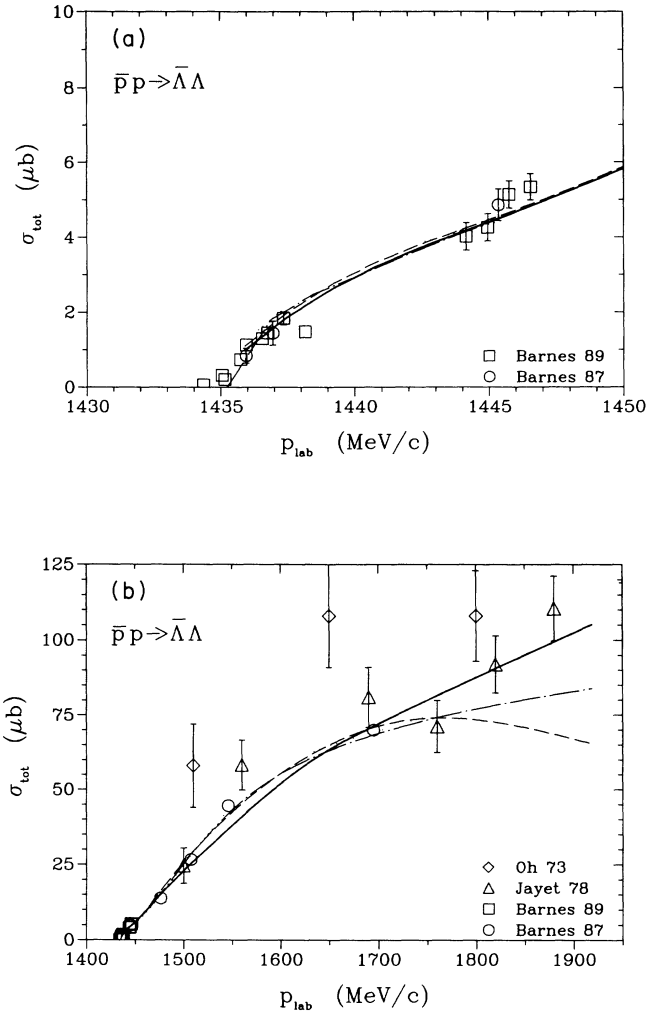

FIG. 3. Total $\bar{p}p\to\bar{\Lambda}\Lambda$ cross sections: (a) near threshold and (b) for intermediate energies. The solid (dashed) line corresponds to the meson-exchange transition model with $K+K^*$ (K) exchange using the $\bar{p}p$ interaction B. The other results originate from the quark-gluon model: The dash-dotted curve is likewise based on the initial-state interaction B whereas, for the dotted curve, initial-state interaction C with increased tensor part is employed. Experimental data are from Ref. [18] (circles), Ref. [19] (squares), Ref. [20] (inverted triangles), and Ref. [21] (triangles).

TABLE II. Parameters of the phenomenological optical potential in the $\bar{\Lambda}\Lambda$ channel for the three different transition models, using the initial-state interaction B. For the quark-gluon model (QG), the numbers in brackets denote the values in case the initial-state interaction C is used.

	$K+K^*$	K	QG	[QG(C)]
U_C	−1142 MeV	−1197 MeV	−898 MeV	[−1339 MeV]
W_C	−1142 MeV	−787 MeV	−866 MeV	[−866 MeV]
U_{LS}	236 MeV	236 MeV	551 MeV	[1575 MeV]
W_{LS}	79 MeV	−236 MeV	−945 MeV	[−945 MeV]
U_T	−1260 MeV fm^{-2}	−1811 MeV fm^{-2}	−2047 MeV fm^2	[−2047 MeV fm^{-2}]
W_T	40 MeV fm^{-2}	−315 MeV fm^{-2}	−157 MeV fm^{-2}	[−40 MeV fm^{-2}]
r_0	0.34 fm	0.24 fm	0.24 fm	[0.20 fm]

meson-exchange transition potentials, respectively, show a somewhat different behavior at very forward and backward angles. Indeed the former tends to overshoot the experiments in either directions. As for the forward direction the same tendency of the differential cross section has been observed in other applications of the constituent-quark model to the $\bar{p}p \to \bar{\Lambda}\Lambda$ transition [9,11,12]. Note that at the highest energy considered here ($p_{\rm lab} = 1695$ MeV/c) such a steep rise at small angles is, in fact, required by the experiment. Here both our meson-exchange transition potentials, but also other models based on meson exchange [2], do have severe difficulties. One has to consider, however, that this energy is already well above the $\bar{\Sigma}^0\Sigma^0$ threshold. An explicit inclusion of this channel might, of course, change the situation. The pronounced enhancement at backward an-

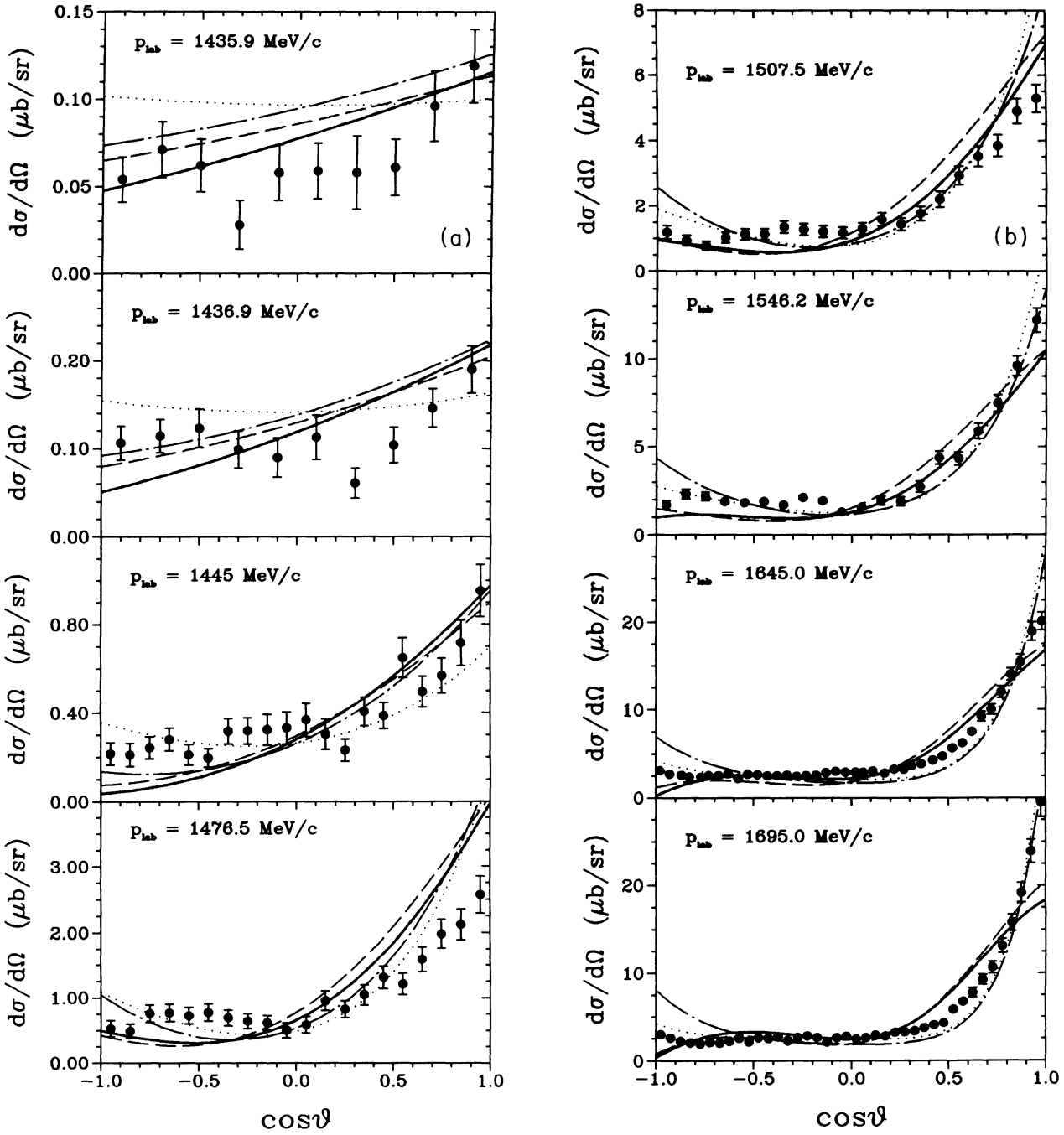

FIG. 4. Differential cross sections for the $\bar{p}p \to \bar{\Lambda}\Lambda$ process. Same description of the curves as in Fig. 3. Experimental data are taken from Ref. [19] ($p_{\rm lab} = 1435.9$, 1436.9, 1445.3 MeV/c), Ref. [18] ($p_{\rm lab} = 1476.5$, 1507.5 MeV/c), Ref. [23] ($p_{\rm lab} = 1546.2$, 1695 MeV/c). The preliminary data for $p_{\rm lab} = 1642$ MeV/c are from Ref. [24].

gles, on the other hand, does not appear in other models based on quark-gluon dynamics [9,11–13]. It is, however, present in the original work of Kohno and Weise [1].

The strongly different characteristics of the involved processes become more explicitly apparent if we now take a look at the contributions of the individual partial waves to the total cross section. From those partial cross sections, listed in Table III for $p_{\rm lab}=1445.3$ and 1546.2 MeV/c, it is immediately evident that in the meson-exchange picture the $\bar{p}p\to\bar{\Lambda}\Lambda$ transition occurs primarily from $L(\bar{p}p)$ to $(L-2)(\bar{\Lambda}\Lambda)$ states, i.e., via a change of the orbital angular momentum by two units [4,6]. At $p_{\rm lab}=1445.3$ MeV/c the results for both meson-exchange models are quite similar: The coherence of the K and K^* exchanges in the tensor channel is obscured by ISI or FSI effects. Indeed, in the Born approximation, the contributions in nondiagonal partial waves are about three times larger for the $K+K^*$ model compared to the K model. This ratio becomes even larger if the same cutoff mass is used at the $N\Lambda K$ vertex.

TABLE III. (Top) partial cross sections (in μb) for the $\bar{p}p\to\bar{\Lambda}\Lambda$ reaction at $p_{\rm lab}=1445.3$ MeV/c. The total empirical cross section is 4.86 ± 0.42 μb. The "experimental" values result from the parametrization of $\sigma_{\rm tot}$ at threshold given in Ref. [19]. (Bottom) partial cross sections (in μb) for the $\bar{p}p\to\bar{\Lambda}\Lambda$ reaction at $p_{\rm lab}=1546.2$ MeV/c. The total empirical cross section is 44.6 ± 1.5 μb.

	$K+K^*$	K	QG	"Experimental"
$^1S_0$	0.19	0.41	0.0	
$^1P_1$	0.04	0.08	0.0	
$^1D_2$	0.0	0.0	0.0	
$^3S_1$	0.53	0.42	1.46	
$^3D_1\to{}^3S_1$	2.07	1.95	1.49	
$^3S_1\to{}^3D_1$	0.0	0.0	0.0	
$^3D_1$	0.01	0.0	0.0	
$^3P_0$	0.18	0.07	0.10	
$^3P_1$	0.04	0.48	1.03	
$^3P_2$	0.15	0.07	0.31	
$^3F_2\to{}^3P_2$	1.24	1.00	0.07	
$^3D_3$	0.0	0.0	0.0	
$^3G_3\to{}^3D_3$	0.03	0.02	0.0	
S	2.79	2.78	2.95	2.84
P	1.65	1.73	1.51	1.73
D	0.04	0.03	0.01	
Total	4.49	4.54	4.47	

	$K+K^*$	K	QG
$^1S_0$	0.22	0.28	0.0
$^1P_1$	0.63	1.23	0.0
$^1D_2$	0.27	0.23	0.0
$^3S_1$	0.52	0.27	0.92
$^3D_1\to{}^3S_1$	2.53	1.51	1.31
$^3S_1\to{}^3D_1$	0.10	0.13	0.08
$^3D_1$	2.08	0.07	0.48
$^3P_0$	3.48	1.93	3.00
$^3P_1$	0.50	9.12	27.75
$^3P_2$	1.69	1.36	5.62
$^3F_2\to{}^3P_2$	15.09	16.45	1.31
$^3D_3$	1.00	0.42	0.69
$^3G_3\to{}^3D_3$	8.05	5.86	0.61
S	3.27	2.06	2.23
P	21.39	30.10	37.68
D	11.54	8.74	1.93
Total	36.8	41.3	42.0

For the QG model the tensor transition amplitudes are identical to zero in the Born approximation. Nonetheless, the corresponding quantities as obtained in our coupled-channel calculation provide the largest contribution to the cross section in the threshold region [cf. the $^3D_1\to{}^3S_1$ transition in Table III (top)]. This clearly demonstrates once again how strong and important ISI and FSI effects are, in particular, at low energies. It also implies that those prescriptions mentioned in the Introduction, where distortions by the ISI and FSI are simply taken into account by multiplying the (on-shell) transition potential matrix element with a constant damping factor [Eq. (1.1)], are totally inadequate. Such prescriptions are, in fact, commonly used in conjunction with quark-gluon-based $\bar{p}p\to\bar{\Lambda}\Lambda$ transition models. In this connection we note that, although the basic transition mechanism on the quark level occurs in the $^3S_1$ partial wave only, all (triplet) waves contribute ultimately to the $\bar{p}p\to\bar{\Lambda}\Lambda$ process.

At $p_{\rm lab}=1546.2$ MeV/c [Table III (bottom)] the cross section of the $K+K^*$ model is dominated by the $^3F_2\to{}^3P_2$ transition (similar to all other models presented in Ref. [6]). In the QG model the largest contribution comes from the $^3P_1$ partial wave. The model with only K exchange has major contributions from both the $^3F_2\to{}^3P_2$ and $^3P_1$ transitions. In general, the tensor transitions are somewhat less pronounced as compared with the $K+K^*$ model. We want to remark that the exceptional behavior of the $^3F_2\to{}^3P_2$ is purely accidental. It can be attributed to the considerably smaller total cross section predicted by the $K+K^*$ model at this particular energy [cf. Table III (bottom)].

Please note that at this energy the D-wave contributions are already significant for the models based on meson exchange, providing about 30% of the total cross section. For the QG model, on the other hand, they contribute only marginally (about 5%). It is obviously the exponential form of the quark-gluon transition potential [Eq. (2.2)] which tends to diminish contributions from higher partial waves. Indeed it seems that this suppression of higher partial waves in the QG model is responsible for the sharp forward peaking of its differential cross section at $p_{\rm lab}=1695$ MeV/c.

Per construction the singlet transitions (i.e., $^1S_0, ^1P_1, ^1D_2, \ldots$) are zero in the QG model, whereas they are small but nonzero in the two meson-exchange models. As we would expect, the corresponding partial-wave cross sections for $K+K^*$ exchange are somewhat smaller than the ones for K exchange.

Finally, we want to compare the model results with

"experimental" S- and P-wave contributions at threshold [19] as they result from fitting the function $\sigma_{\text{tot}}=b_0\epsilon^{1/2}+b_1\epsilon^{3/2}$ (with the excess energy $\epsilon=\sqrt{s}-m_\Lambda-m_{\bar\Lambda}$ and $b_0=1.51$ μb/MeV$^{1/2}$, $b_1=0.26$ μb/MeV$^{3/2}$) to the empirical cross sections. These values are given in column 4 of Table III (top). The predictions of all three models agree quite well with them. Note that this is by no means trivial. As has been pointed out already in Ref. [6], the K-exchange model of Ref. [1] as well as the model of Ref. [2] show very different behaviors, the former having a S- to P-wave splitting of 1.95–2.8 μb at $p_{\text{lab}}=1445.3$ MeV/c while it is 3.95–0.95 for the latter. Since in our case different models for the $\bar pp\to\bar\Lambda\Lambda$ transition lead to rather similar results, we are led to the conclusion that the S- and P-wave contributions at threshold are primarily determined by the ISI and FSI employed.

B. Polarizations

In the analysis above we observed that the individual partial waves contribute rather differently to the cross

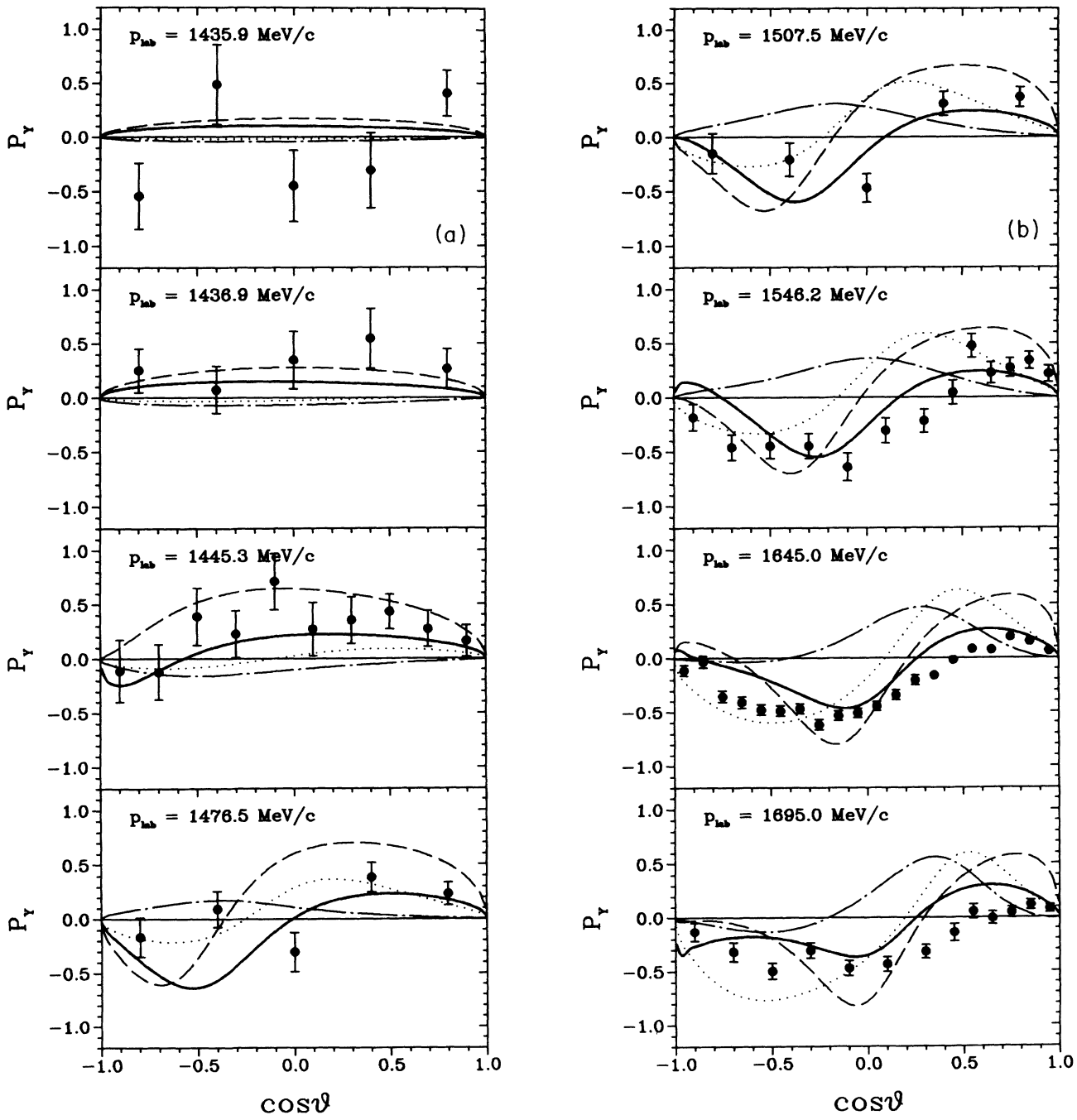

FIG. 5. Polarizations for the $\bar pp\to\bar\Lambda\Lambda$ process. Same description as in Fig. 4.

section for the three transition models under examination. Consequently, we expect to see more pronounced effects from the different transition mechanisms in those observables which depend more specifically on particular partial waves. Hence, we now take a closer look at the polarizations and, in the next subsections, at other $\bar{p}p \to \bar{\Lambda}\Lambda$ spin observables.

The polarizations predicted by the three transition interactions are shown in Fig. 5. Both models based on meson exchange reproduce qualitatively the experimental angular distributions [18,19,23,24] over the whole energy range considered, with the $K+K^*$ model providing a somewhat better description. The quark-gluon model, on the other hand, produces a rather different pattern, in striking disagreement with the data.

However, before any premature conclusions are drawn we would like to remind the reader on the strong sensitivity of these polarizations to the ISI and FSI found in our earlier paper [6]. Besides the $K+K^*$ interaction used in the present paper, we have considered there an alternative $K+K^*$ model with another initial-state interaction (A), in which both the spin-orbit and tensor terms in

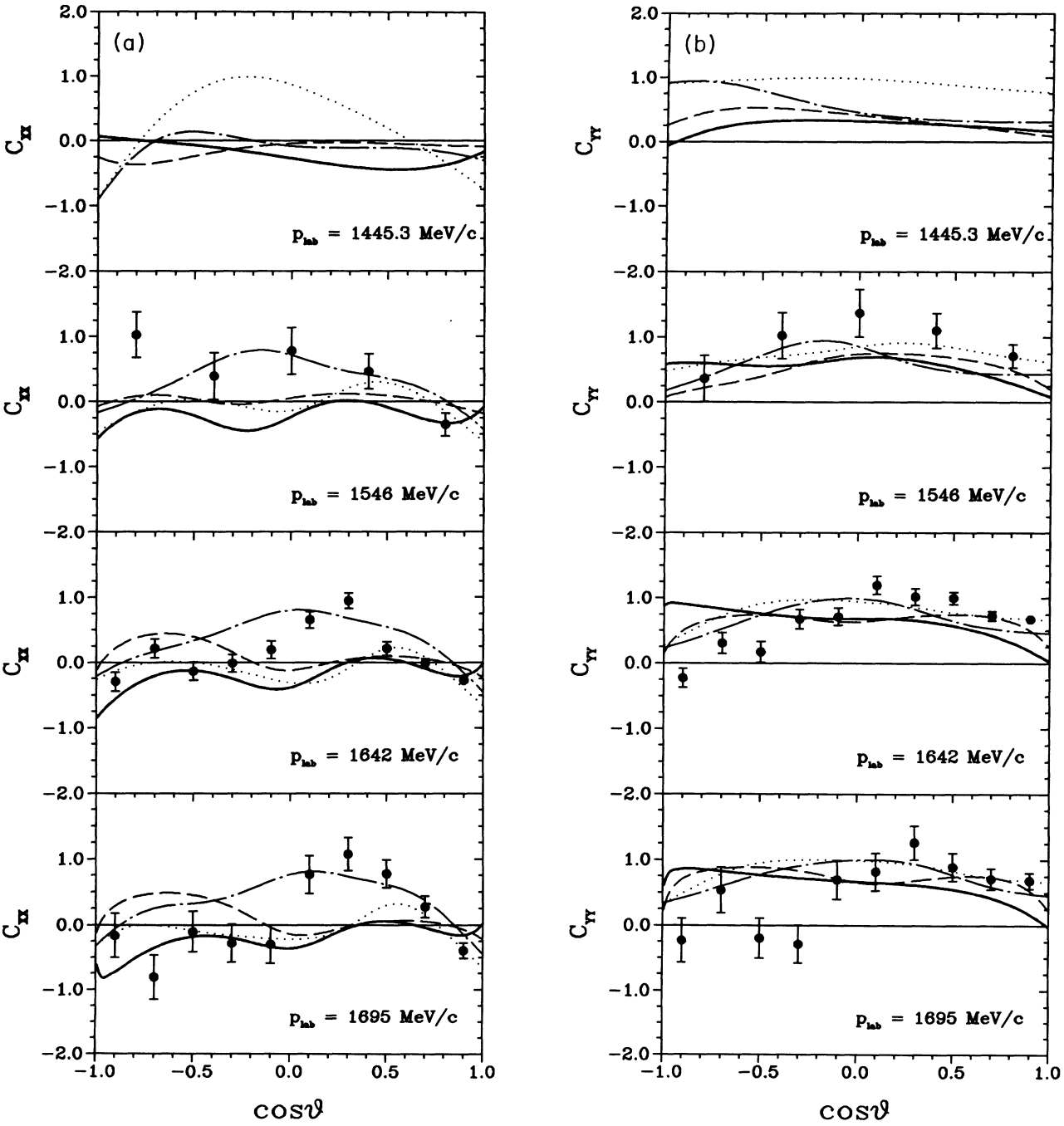

FIG. 6. Spin-correlation parameter for the $\bar{p}p \to \bar{\Lambda}\Lambda$ process. Same description of the curves as in Fig. 3. Experimental data are taken from Ref. [23] ($p_{lab} = 1546.2$, 1695.0 MeV/c). The preliminary data for $p_{lab} = 1642$ MeV/c are from Ref. [24].

the annihilation part have been omitted. This (short-range) modification of the ISI had little influence on the cross sections but led to a considerable change in the predicted polarizations. The same is true for the quark-gluon transition model. Using ISI C instead of B and readjusting the parameters in the final-state interaction (see Table II), Fig. 5 shows drastic differences in the polarizations, the results with C being much more similar to the empirical situation. Indeed, it should be noted that the original application of the quark-gluon model in Ref. [1], with suitable though quite different initial- and final-state interactions than used here, yielded good agreement with the polarization data at $p_{\text{lab}}=1508$ MeV/c.

C. Spin-correlation parameters

Results for the spin-correlation parameters are presented in Fig. 6 at four energies. Measurements have been published so far for $p_{\text{lab}}=1546.2$ and 1695 MeV/c [23], and data for $p_{\text{lab}}=1642$ MeV/c are already in preparation [24,25]. Because of charge conjugation invariance $C_{zx}=C_{xz}$ and because of parity conservation $C_{xy}=C_{yx}=C_{yz}=C_{zy}=0$.

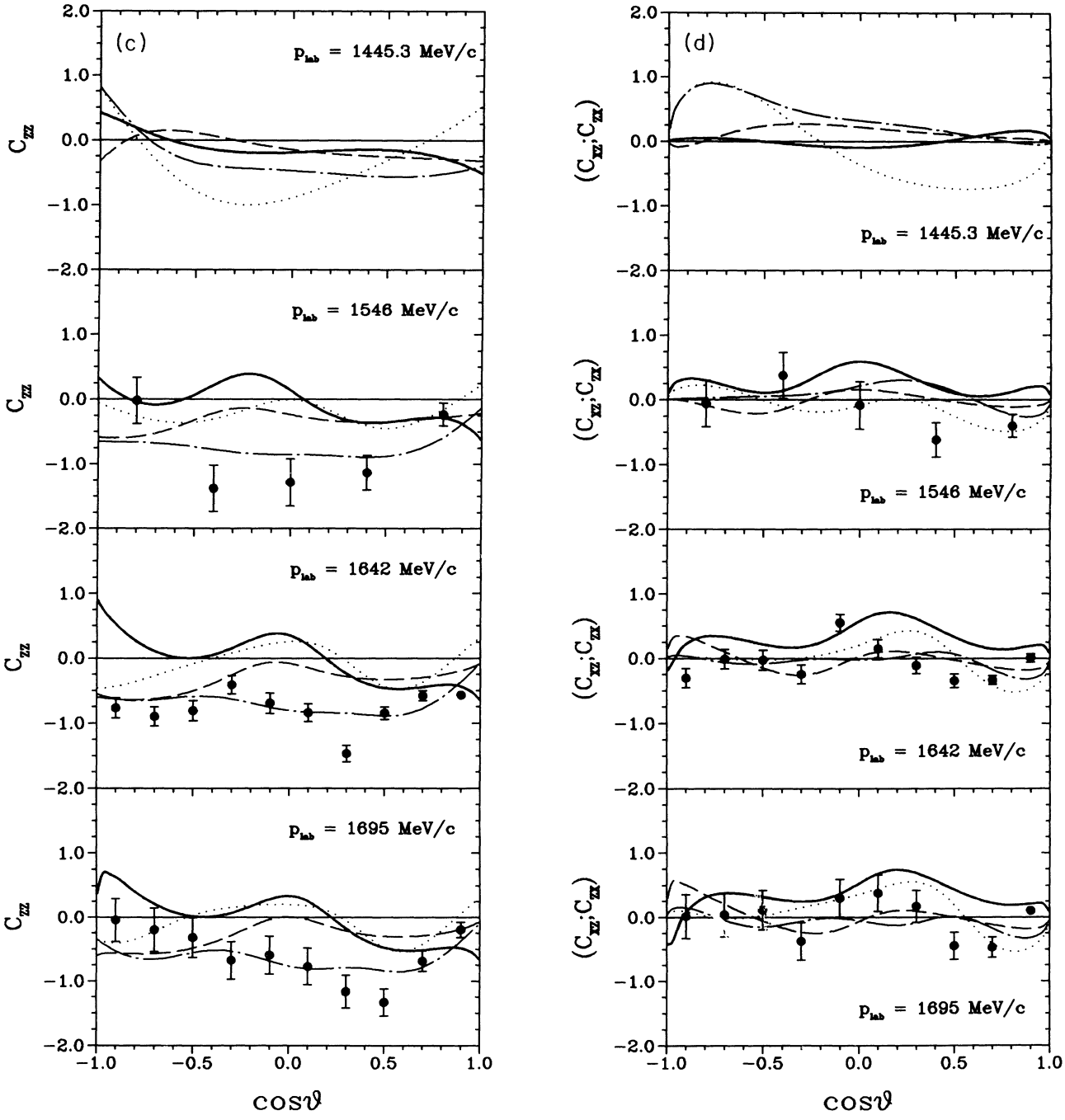

FIG. 6. (*Continued*).

For C_{xx} and C_{zz}, there are sizable differences in the model predictions at higher energies and nonforward directions. As in the case of the polarization, the angular dependence nevertheless exhibits a similar trend for both meson-exchange models whereas the quark-gluon model provides a completely different pattern, which, especially in the forward direction, seems to be in better agreement with the empirical analysis. At this point, however, the following remarks should be made: First, several empirical values lies well beyond physical bounds $\{-1,+1\}$; second, the data (at $p_{\rm lab}=1546.2$ MeV/c as well as at $p_{\rm lab}=1642$ MeV/c) do not satisfy the relation $C_{xx}=-C_{yy}$ at backward angles as required by rotational invariance; third, the above constraints due to parity conservation have not yet been imposed and are, in fact, badly violated by the present empirical analysis. Therefore, the empirical data should be viewed with caution. Indeed, from the ongoing analysis of new data at $p_{\rm lab}=1918$ MeV/c [24,26], it is known that in applying those constraints from the beginning, the empirical values for some of the C_{ij} change substantially [27]. It would be worthwhile to repeat the analysis at the energies shown in the figures. For $(C_{xz};C_{zx})$, and even more for C_{yy}, on the other hand, all models provide rather similar results, in qualitative agreement with the data.

Figure 7 contains the resulting singlet fraction

$$F_S=\tfrac{1}{4}(1-\langle\sigma_1\cdot\sigma_2\rangle)=\tfrac{1}{4}(1+C_{xx}-C_{yy}+C_{zz})\ .$$

This observable is exactly zero for the QG model and quite small for both meson-exchange models. Per definition, its value is ranged between 0 and 1 and cannot be negative. This shows again that the present analysis of the empirical data should be viewed with caution.

As for the polarization, the spin-correlation parameters depend on the kind of initial- and final-state interactions used. This is again documented for the QG model by giving in addition the results for the initial-state interaction C. As seen from Eq. (A5), C_{ij} depend strongly on the tensor-type amplitudes. Indeed, it is the additional tensor-type interaction in the annihilation part of model C which is responsible for the remarkable shift (it is somewhat less pronounced in C_{yy}, probably because it depends on the square of amplitudes only [see Eq. (A5)]; the differences are much smaller if the initial-state interaction A (defined in Ref. [6]), having no tensor term in the optical potential, is used. This has been demonstrated for the $K+K^*$ model in Ref. [6].

We conclude that the results for the spin-correlation parameters with the exception of C_{yy} depend on the ISI and FSI. Therefore, given the present theoretical uncertainties in the ISI and FSI, these observables also do not seem to be suitable to distinguish between different transition scenarios. Although C_{yy} has proven to be quite stable against variations of the ISI and FSI, it cannot discriminate either since, as we have seen before, the results for this observable predicted by different transition models turn out to be quite similar.

D. Spin-transfer observables

As discussed before, in the meson-exchange model the transition occurs primarily via a change of orbital angular momentum by two units (see Table III). This requires that the spin projection of the total spin (spin-triplet configuration) is flipped. For the $\bar{p}p\to\bar{\Lambda}\Lambda$ interaction derived from the constituent-quark model, on the other hand, this spin flip is very small because of the weak ($^3P_0$) or even vanishing ($^3S_1$) tensor component of the transition operator. Therefore, spin-transfer observables like D_{nn} or K_{nn} should be suitable to discriminate between these transition models.

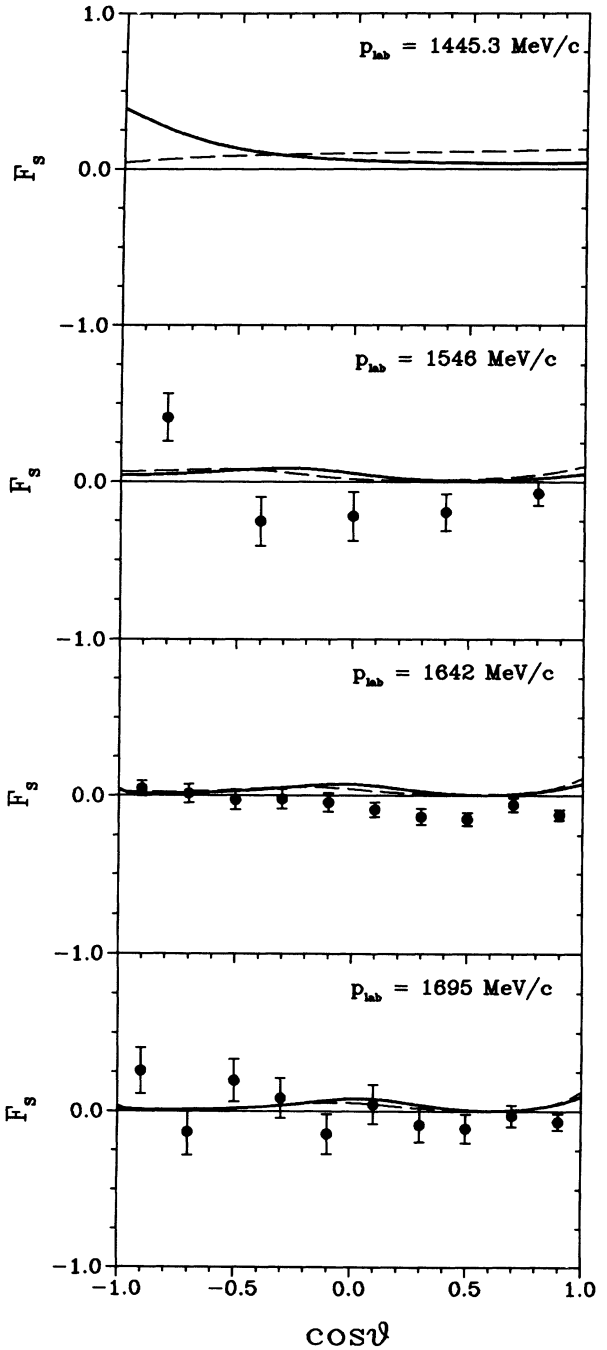

FIG. 7. Singlet fraction F_s for the $\bar{p}p\to\bar{\Lambda}\Lambda$ process. Same description as in Fig. 6. F_s is exactly zero for the quark-gluon transition model.

Let us start with the depolarization parameter D_{nn}, which describes the spin transfer from the target to the recoil particle. With the usual parametrization of the spin-scattering matrix (see the Appendix), the amount of spin flip of the one-particle spin, characterized by $1-D_{nn}$, is given by

$$\frac{d\sigma}{d\Omega}(1-D_{nn})=\frac{q'}{q}(|c|^2+|d|^2+|g|^2)\ . \tag{3.1}$$

Note that maximal spin flip, i.e., $D_{nn}=-1$, is generated by a pure tensor interaction. On the other hand, the simple constituent-quark model (in the $^3S_1$ version) yields (in Born approximation) $D_{nn}=\frac{2}{3}$, i.e., small spin flip, which is generated by the spin dependence of the projection operator $P_T=\frac{1}{4}(3+\sigma_1\cdot\sigma_2)$ on spin-triplet states. Figure 8 shows the full results of the coupled-channel calculation, at three selected energies. Obviously, the initial- and final-state interactions modify the amount of spin flip; however, most importantly, the strong differences obtained from the basic transition mechanisms persists:

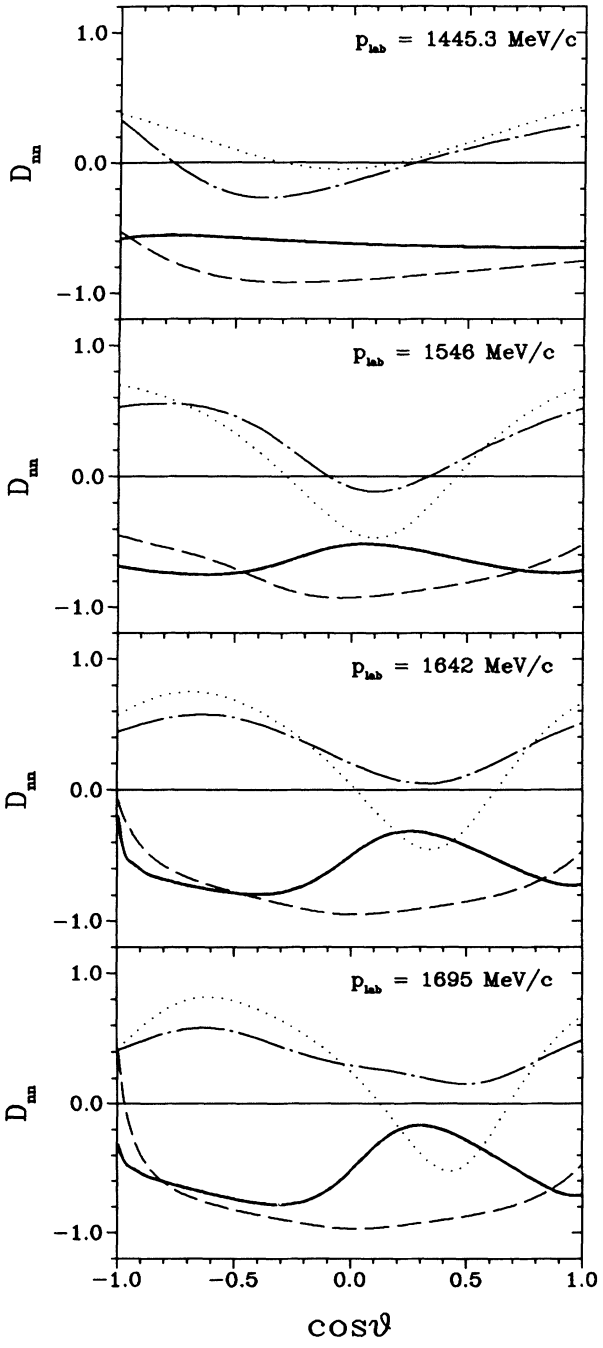

FIG. 8. Depolarization D_{nn} for the $\bar{p}p\to\bar{\Lambda}\Lambda$ process. Same description of the curves as in Fig. 3.

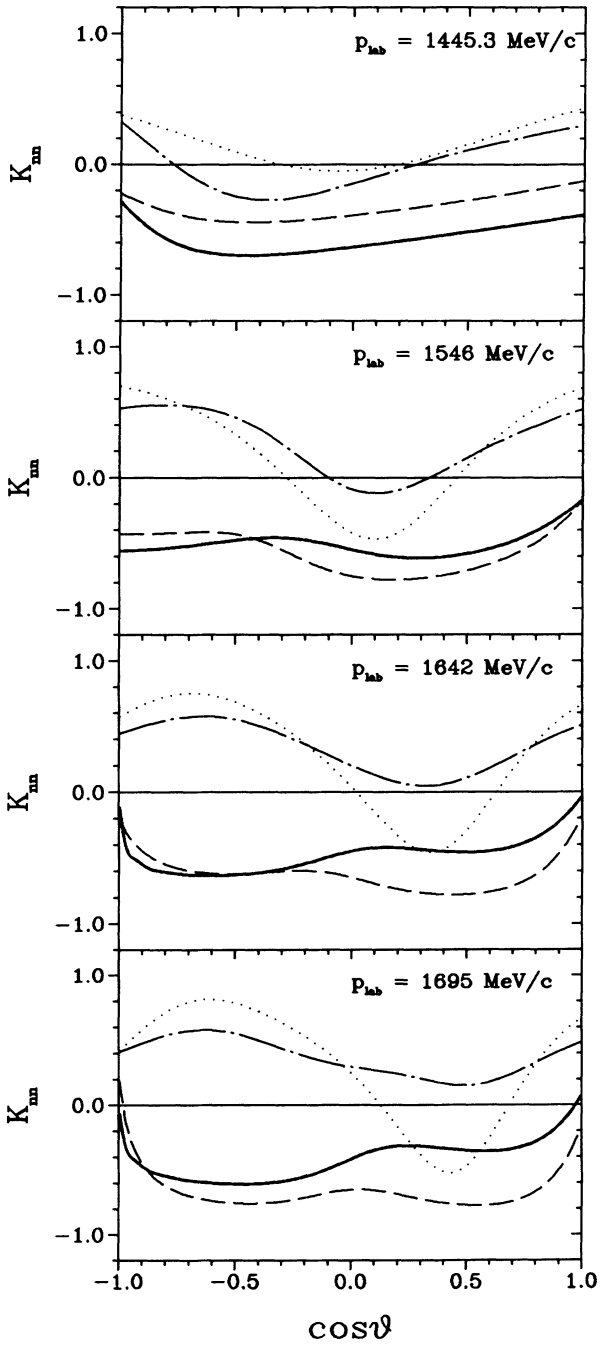

FIG. 9. Polarization-transfer observable K_{nn} for the $\bar{p}p\to\bar{\Lambda}\Lambda$ process. Same description of the curves as in Fig. 3.

$(K+K^*)$- and K-exchange models lead to a much larger spin transfer than the constituent-quark model, throughout the whole angular range. Moreover, the results are quite stable against variations of the ISI and FSI: As shown in Fig. 8, the large difference between meson- and quark-gluon model predictions essentially remains even when we employ, for the case of the QG model, ISI C having a strong additional tensor part in the optical potential.

Next let us consider the polarization transfer observable K_{nn}, which measures the spin transfer from the target to the scattered particle. Here, Fig. 9 shows that the possibility for discriminating between the models is somewhat reduced in the forward direction. In general, the meson-exchange models have a less pronounced angular dependence and deviate from the constituent-quark model especially in the backward direction. At threshold, the K-exchange model results lie between those of the constituent-quark model and the $(K+K^*)$ model. Again, the results are quite stable against variations of the ISI and FSI, especially in forward and backward directions.

Finally, we also want to present corresponding results for the other angular combinations of the spin-transfer observables, i.e., D_{xx},D_{zz},D_{xz} (Fig. 10) and K_{xx},K_{zz},K_{xz} (Fig. 11), at one selected energy. Obviously, the differences between the various model predictions are somewhat smaller compared to those observed for D_{nn} $(\equiv D_{yy})$.

Thus, it appears that the depolarization parameter D_{nn} is most suitable for discriminating between meson-exchange and simple constituent-quark models for the $\bar{p}p \to \bar{\Lambda}\Lambda$ transition.

IV. SUMMARY

In this paper, we have investigated various models for the $\bar{p}p \to \bar{\Lambda}\Lambda$ transition process. This was done in a full

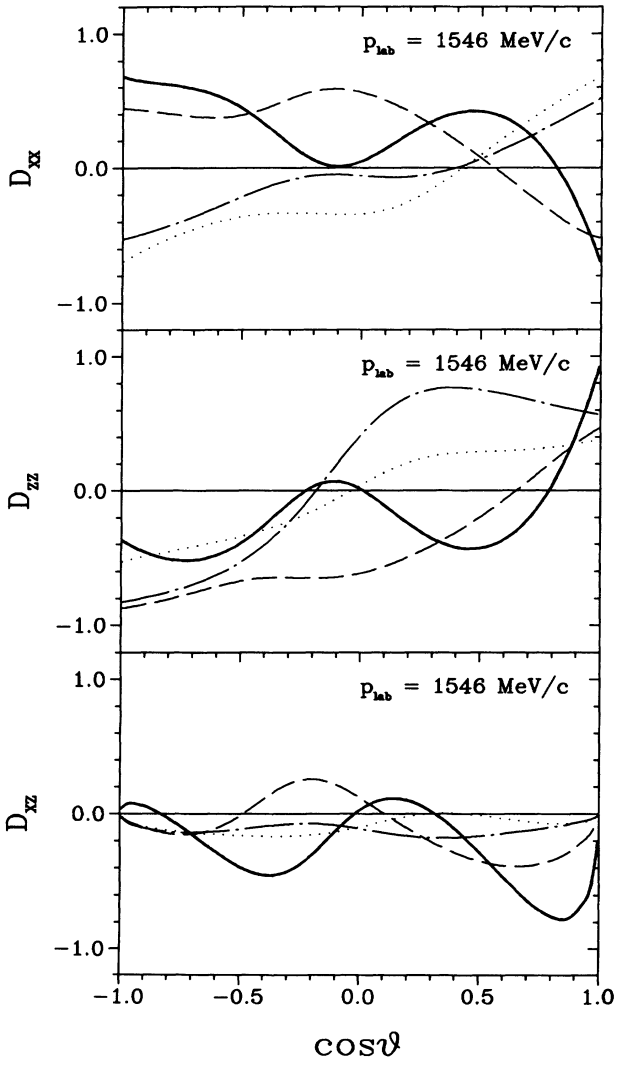

FIG. 10. Depolarization parameters D_{xx},D_{zz},D_{xz} for the $\bar{p}p \to \bar{\Lambda}\Lambda$ process. Same description of the curves as in Fig. 3.

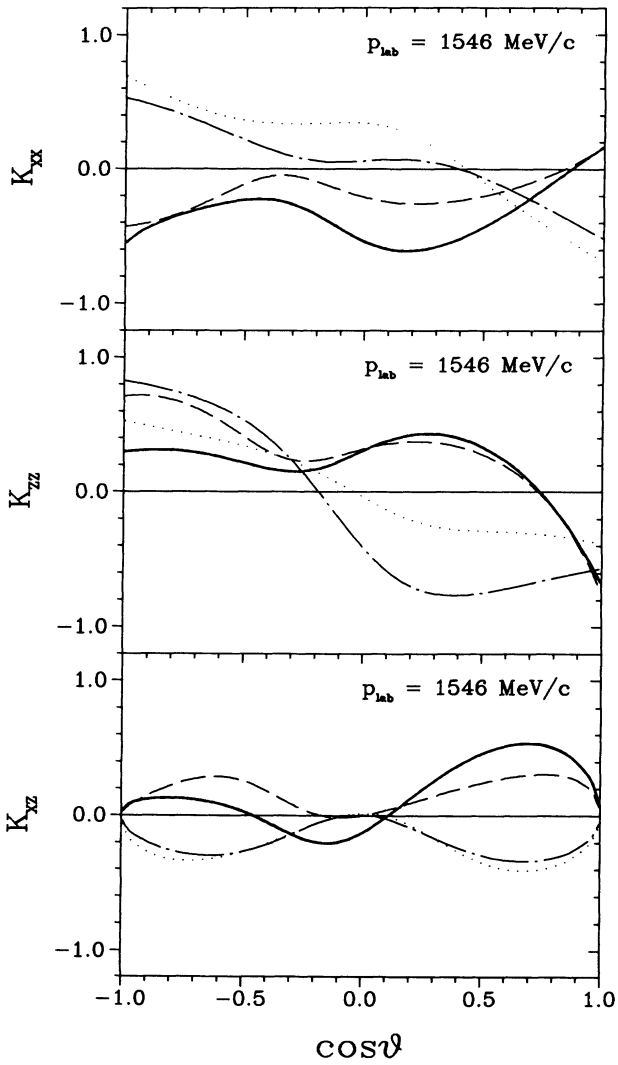

FIG. 11. Polarization-transfer parameters K_{xx},K_{zz},K_{xz} for the $\bar{p}p \to \bar{\Lambda}\Lambda$ process. Same description of the curves as in Fig. 3.

coupled-channel ($\bar{p}p, \bar{\Lambda}\Lambda$) calculation to study the effects of distortions in the initial as well as the final channel. The first transition model was based on $K+K^*$ exchange: It was possible to take both coupling constants and cutoff masses to be precisely the same as in our hyperon-nucleon model [16], i.e., no additional, *ad hoc* regularization was introduced. In case of the K-exchange model, the cutoff mass $\Lambda_{N\Lambda K}$ had to be increased from 1.2 to 1.7 GeV in order to (roughly) account for the missing strength in the tensor channel generated by K^* exchange. Finally, for the $^3S_1$ version of the constituent-quark model, the effective coupling strength had to be increased in our coupled-channel calculation by about 60% in comparison to the value used in the DWBA calculation of Ref. [1].

Throughout, the same elastic interaction in the initial as well as the final channel was used. They have been derived from one-boson-exchange versions of the Bonn NN potential and a corresponding extension to the hyperon-nucleon case [16]. Annihilation (containing both a real and an imaginary part) is parametrized by a phenomenological optical potential of Gaussian form. For $\bar{p}p$, the parameters are independent of the $\bar{\Lambda}\Lambda$ channel adjusted to fit the total, integrated elastic, and charge-exchange cross sections in the energy range relevant for the $\bar{\Lambda}\Lambda$ production. The annihilation parameters in the $\bar{\Lambda}\Lambda$ channel represent the only free parameters of our model and have been adjusted separately for each transition model to the $\bar{p}p \to \bar{\Lambda}\Lambda$ cross sections. All models reproduce the total and differential cross sections with reasonable accuracy. Sizable differences occur in the description of polarizations. Whereas both meson-exchange models are able to account for the qualitative trend of the data, with the $K+K^*$ model giving the best agreement, the quark-gluon model shows a completely different pattern, in striking disagreement with experiment. However, polarizations are known to be extremely sensitive to the treatment of initial- and final-state distortions (cf. Ref. [6]). Indeed, with a suitable modification of the initial-state interaction, polarization data can also be satisfactorily reproduced within the quark-gluon model.

Similar differences have been observed in the spin-correlation parameters C_{ij}, especially in C_{xx} and C_{zz}. Again, the quark-gluon model leads to a completely different pattern, which, in fact, seems to be in better agreement with the data. The reader should be aware of the fact, however, that the present analysis of corresponding empirical data leads to values outside of physical bounds. (One reason is probably that up to now basic constraints due to parity conservation and charge-conjugation invariance of the strong interaction have not been imposed on the analysis). Therefore, the present empirical values are to be taken with some care and it is certainly premature to conclude that empirical spin-correlation data definitely favor the quark-gluon model. Certainly, it would be worthwhile to improve the present analysis. In any case, since also the description of the spin-correlation observables depends considerably on the choice of the ISI and FSI, it is certainly difficult to draw conclusions about the basic transition mechanism from the spin-correlation parameters.

The situation is dramatically different when investigating the spin-transfer observables: In the meson-exchange model, the transition process is dominated by nondiagonal tensor transitions like $^3F_2 \to {}^3P_2$, which require a flip of the spin projection of the total spin. In contrast, the quark-gluon model leads mostly to diagonal transitions conserving the orbital angular momentum (e.g., $^3P_1 \to {}^3P_1$), which can occur without any spin flip. Indeed, there is a large difference between the predictions for the depolarization parameter D_{nn}. Moreover, the results are remarkably stable against variations of the ISI and FSI. Therefore, we strongly feel that a measurement of the depolarization D_{nn}, if done with reasonable accuracy, should be able to discriminate between different transition models based on either meson- or one-gluon exchange.

Of course, if D_{nn} measurements definitely favor the description in terms of collective degrees of freedom, i.e., baryons and mesons, the QCD-inspired models could always be extended to include multigluon exchanges. In this way, rough equivalence with the meson-exchange results might be achieved. However, the nice feature of these models, namely, their striking simplicity, would then be gone.

ACKNOWLEDGMENTS

We thank K. Kilian and W. Oelert for many discussions, especially about details of the analysis of the empirical spin-correlation parameters. One of us (J.H.) would like to thank the Institut für Kernphysik of the Forschungszentrum Jülich for the hospitality during his visit. This work was partly supported by the Australian Research Council.

APPENDIX

For the $\bar{p}p \to \bar{\Lambda}\Lambda$ process, the spin-scattering matrix can be parametrized as [28]

$$M = \tfrac{1}{2}[(a+b)I + (a-b)\boldsymbol{\sigma}_1\cdot\hat{\mathbf{n}}\,\boldsymbol{\sigma}_2\cdot\hat{\mathbf{n}} + (c+d)\boldsymbol{\sigma}_1\cdot\hat{\mathbf{k}}\,\boldsymbol{\sigma}_2\cdot\hat{\mathbf{k}} + (c-d)\boldsymbol{\sigma}_1\cdot\hat{\mathbf{P}}\boldsymbol{\sigma}_2\cdot\hat{\mathbf{P}} + e(\boldsymbol{\sigma}_1+\boldsymbol{\sigma}_2)\cdot\hat{\mathbf{n}} + g(\boldsymbol{\sigma}_1\cdot\hat{\mathbf{k}}\boldsymbol{\sigma}_2\cdot\hat{\mathbf{P}} + \boldsymbol{\sigma}_1\cdot\hat{\mathbf{P}}\boldsymbol{\sigma}_2\cdot\hat{\mathbf{k}})] , \tag{A1}$$

with

$$\hat{\mathbf{P}} = \frac{\mathbf{q}'}{|\mathbf{q}'|} , \quad \hat{\mathbf{n}} = \frac{\mathbf{q}\times\mathbf{q}'}{|\mathbf{q}\times\mathbf{q}'|} , \quad \hat{\mathbf{k}} = \hat{\mathbf{n}}\times\hat{\mathbf{P}} , \tag{A2}$$

and $\mathbf{q}$ ($\mathbf{q}'$) being the c.m. momentum in the initial (final) channel. We then obtain for the differential cross section

$$\frac{d\sigma}{d\Omega} \equiv I_0 = \frac{q'}{q}\frac{1}{4}\mathrm{tr}(MM^\dagger) = \frac{1}{2}\frac{q'}{q}(|a|^2+|b|^2+|c|^2+|d|^2+|e|^2+|g|^2) , \tag{A3}$$

for the polarization

$$P_Y^{\Lambda}=\frac{\mathrm{tr}(\sigma_Y^{\Lambda}MM^{\dagger})}{\mathrm{tr}(MM^{\dagger})}$$
$$=\frac{q'}{q}\frac{1}{I_0}[\mathrm{Re}(ae^*)+\mathrm{Im}(dg^*)]\ , \tag{A4}$$

and for the spin-correlation parameters

$$C_{ij}=\frac{\mathrm{tr}(\sigma_i^{\Lambda}\sigma_j^{\bar{\Lambda}}MM^{\dagger})}{\mathrm{tr}(MM^{\dagger})}\ ,$$
$$C_{xx}=-\frac{q'}{q}\frac{1}{I_0}[\mathrm{Re}(ad^*+bc^*)+\mathrm{Im}(ge^*)]\ ,$$
$$C_{yy}=\frac{1}{2}\frac{q'}{q}\frac{1}{I_0}(|a|^2-|b|^2-|c|^2+|d|^2+|e|^2+|g|^2)\ , \tag{A5}$$
$$C_{zz}=\frac{q'}{q}\frac{1}{I_0}[\mathrm{Re}(ad^*-bc^*)+\mathrm{Im}(ge^*)]\ ,$$
$$C_{xz}=-\frac{q'}{q}\frac{1}{I_0}[\mathrm{Re}(ag^*)+\mathrm{Im}(ed^*)]\ .$$

Finally, the spin-transfer parameters are given by

$$D_{ij}=\frac{\mathrm{tr}(\sigma_i^{\Lambda}M\sigma_j^{p}M^{\dagger})}{\mathrm{tr}(MM^{\dagger})}\ ,$$
$$D_{nn}=\frac{1}{2}\frac{q'}{q}\frac{1}{I_0}(|a|^2+|b|^2-|c|^2-|d|^2+|e|^2-|g|^2)\ ,$$
$$D_{xx}=-\frac{q'}{q}\frac{1}{I_0}\mathrm{Re}(ab^*+cd^*)\ , \tag{A6}$$
$$D_{zz}=-\frac{q'}{q}\frac{1}{I_0}\mathrm{Re}(ab^*-cd^*)\ ,$$
$$D_{xz}=\frac{q'}{q}\frac{1}{I_0}[\mathrm{Re}(cg^*)+\mathrm{Im}(be^*)]\ ,$$

and

$$K_{ij}=\frac{\mathrm{tr}(\sigma_i^{\bar{\Lambda}}M\sigma_j^{p}M^{\dagger})}{\mathrm{tr}(MM^{\dagger})}\ ,$$
$$K_{nn}=\frac{1}{2}\frac{q'}{q}\frac{1}{I_0}(|a|^2-|b|^2+|c|^2-|d|^2+|e|^2-|g|^2)\ ,$$
$$K_{xx}=-\frac{q'}{q}\frac{1}{I_0}\mathrm{Re}(ac^*+bd^*)\ , \tag{A7}$$
$$K_{zz}=-\frac{q'}{q}\frac{1}{I_0}\mathrm{Re}(ac^*-bd^*)\ ,$$
$$K_{xz}=-\frac{q'}{q}\frac{1}{I_0}[\mathrm{Re}(bg^*)+\mathrm{Im}(ec^*)]\ .$$

[1] M. Kohno and W. Weise, Phys. Lett. **179B**, 15 (1986); **206B**, 584 (1988); Nucl. Phys. A**479**, 433c (1988).

[2] P. LaFrance, B. Loiseau, and R. Vinh Mau, Phys. Lett. B **214**, 317 (1988); P. LaFrance and B. Loiseau, Nucl. Phys. **A528**, 557 (1991).

[3] J. A. Niskanen, University of Helsinki Report HU-TFT-85-28, 1985.

[4] R. G. E. Timmermans, T. A. Rijken, and J. J. de Swart, Nucl. Phys. **A479**, 383c (1988); Phys. Rev. D **45**, 2288 (1992).

[5] F. Tabakin and R. A. Eisenstein, Phys. Rev. C **31**, 1857 (1985); F. Tabakin, R. A. Eisenstein, and Y. Lu, *ibid.* **44**, 1749 (1991).

[6] J. Haidenbauer, T. Hippchen, K. Holinde, B. Holzenkamp, V. Mull, and J. Speth, Phys. Rev. C **45**, 931 (1992).

[7] H. Genz and S. Tatur, Phys. Rev. D **30**, 63 (1984); G. Brix, H. Genz, and S. Tatur, *ibid.* **39**, 2054 (1989); H. Genz, M. Nowakowski, and D. Woitschitzky, Phys. Lett. B **260**, 179 (1991).

[8] H. R. Rubinstein and H. Snellman, Phys. Lett. **165B**, 187 (1985).

[9] S. Furui and A. Fässler, Nucl. Phys. **A468**, 669 (1987); A. Fässler, Prog. Part. Nucl. Phys. **30**, 295 (1988).

[10] P. Kroll and W. Schweiger, Nucl. Phys. **A474**, 608 (1987); P. Kroll, B. Quadder, and W. Schweiger, *ibid.* **B316**, 373 (1989).

[11] M. A. Alberg, E. M. Henley, and L. Wilets, Phys. Rev. C **38**, 1506 (1988); Z. Phys. A **331**, 207 (1988); M. A. Alberg, E. M. Henley, L. Wilets, and P. D. Kunz, Nucl. Phys. **A508**, 323c (1990); in *Proceedings of the First Biennial Conference on Low Energy Antiproton Physics, LEAP 90,* edited by P. Carlson, A. Kerek, and S. Szilagyi (World Scientific, Singapore, 1991), p. 129.

[12] M. Burkardt and M. Dillig, Phys. Rev. C **37**, 1362 (1988).

[13] W. Roberts, Z. Phys. C **49**, 633 (1991).

[14] J. Haidenbauer, K. Holinde, and M. B. Johnson, Phys. Rev. C **45**, 2055 (1992).

[15] R. Machleidt, K. Holinde, and Ch. Elster, Phys. Rep. **149**, 1 (1987).

[16] B. Holzenkamp, K. Holinde, and J. Speth, Nucl. Phys. **A500**, 485 (1989).

[17] M. Kohno and W. Weise, Nucl. Phys. **A454**, 429 (1986).

[18] P. D. Barnes *et al.*, Phys. Lett. B **189**, 249 (1987).

[19] P. D. Barnes *et al.*, Phys. Lett. B **229**, 432 (1989).

[20] B. Jayet *et al.*, Il Nuovo Cimento A **45**, 371 (1978).

[21] B. Y. Oh *et al.*, Nucl. Phys. **B51**, 57 (1973).

[22] R. G. E. Timmermans, Ph.D. thesis, Nijmegen, 1991.

[23] P. D. Barnes *et al.*, Nucl. Phys. **A526**, 575 (1991).

[24] T. Johansson *et al.*, in *Proceedings of the First Biennial Conference on Low Energy Antiproton Physics, LEAP 90* [11], p. 192.

[25] H. Fischer, Ph.D. thesis, University of Freiburg, Germany.

[26] M. Ziolkowski, Ph.D. thesis, University of Cracow, Poland.

[27] M. Ziolkowski (private communication).

[28] J. Bystricky, F. Lehar, and P. Winternitz, J. Phys. (Paris) **39**, 1 (1978); P. LaFrance and P. Winternitz, *ibid.* **41**, 1391 (1980).